Damage and cracking of synthetic and natural glasses subjected to triaxial deformation

Audrey OUGIER-SIMONIN*, Yves GUEGUEN, Jérôme FORTIN & Alexandre SCHUBNEL

Laboratoire de Géologie de l'Ecole normale supérieure - UMR CNRS 8538 - 24 rue Lhomond 75231 Paris, FRANCE

*contact : ougier@geolgie.ens.fr

1. Introduction

Crack initiation and growth in brittle solids under tension have been extensively studied by experimental, theoretical and numerical approaches. It has been established that dynamic brittle fracture is related to fundamental physical parameters and processes, such as crack speed, crack branching, surface roughening, and dynamic instabilities. On the other hand, less studies have been done in the area of compressive fracture despite its vital importance in geology, material science and engineering applications (such as the improvement and the insurance of the nuclear wastes storage).

The present work aims to investigate thermo-mechanical cracking effects on elastic wave velocities, mechanical strength and permeability under pressure to evaluate damage evolution, brittle failure and transport properties on a synthetic glass (SON 68), and to hightlight the very different behavior of the glass amorphous structure compared to any rock structure.

2. Microstructural observations

Original synthetic glass (OG)

Fig.1: *OG texture observed with a SEM.*

- Very homogeneous microstructure with almost non existent porosity (isotropic glass)
- Small clusters of platinoids (blank minerals)
- density = 2.8 ± 0.01, porosity = 0 %
- $E_{dynamic}$ = 84 GPa, $\nu_{dynamic}$ = 0.25

Thermal treated glass (TT)

Thermal treatment protocol

Heating	+ Thermal shock
from T_A (20°C) to T_H (100, 200, 300 °C)	$\Delta T = \frac{T_H - T_A}{\Delta t}$
~15 hours	+ 5 sec.

TT glasses

- Homogeneous distribution with randomly oriented cracks (isotropic cracked glass)
- 0.2 < crack porosity < 0.24 %
- 56 < $E_{dynamic}$ < 84 GPa
- 0.24 < $\nu_{dynamic}$ < 0.29

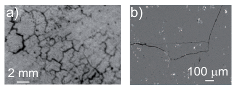

Fig. 2: *Cracks in TT samples: a) surface pattern photo; b) SEM view.*

Seljadur basalt (SB)

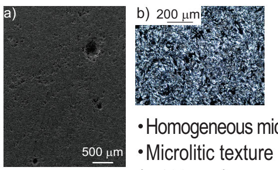

Fig. 3: *SB texture observed with : a)S.E.M; b) optical microscope.*

- Homogeneous microstructure with few gas bubbles
- Microlitic texture similar with very small grains (< 100 mm)
- density = 2.9 ± 0.02, porosity ~ 5%
- $E_{dynamic}$ = 83 GPa, $\nu_{dynamic}$ = 0.32

3. Experimental setup

Sample assembly

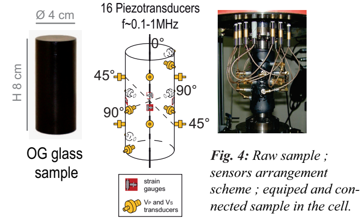

Fig. 4: *Raw sample ; sensors arrangement scheme ; equiped and connected sample in the cell.*

Triaxial cell apparatus

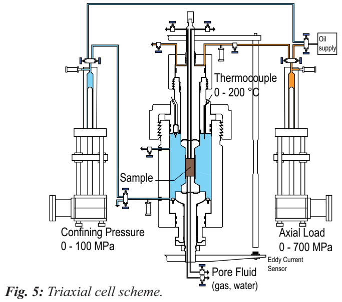

Fig. 5: *Triaxial cell scheme.*

- Induce the change of the glass symmetry originally ISO to a TI symmetry
- Reproduce *in situ* stress field for nuclear waste packages in geological storage.

Ultrasonic data acquisition

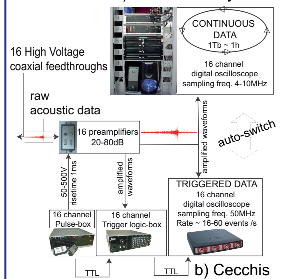

- Count and localization of microcracking events
- Crack propagation monitoring

Fig. 6: *Ultrasonic signal emitting-recording system : a) acoustic emission system (passive mode); b) elastic wave velocity system (active mode).*

Experimental conditions

Temperature for all tests:	20°C
(1) Dry hydrostatic tests	
Pressure:	0-50 MPa
(2) Dry deviatoric tests	
Confining pressure P_{conf}:	15 MPa
Axial stress σ_1:	up to failure
(3) Saturated hydrostatic tests	
Fluid pressure P_f:	5 MPa
Effective pressure P_{eff}:	0-20 MPa

4. Elastic wave velocities, mechanical behavior, damage monitoring and permeability investigations

Hydrostatic data

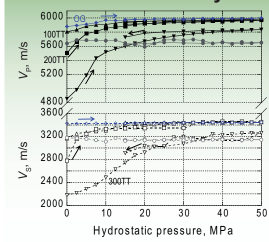

Fig. 7: *P- and S- wave velocities recorded under hydrostatic loading.*

- OG and SB are isotropic materials
- Crack closure is observed at P ~ 15 MPa (ξ=10^{-4}-10^{-3})

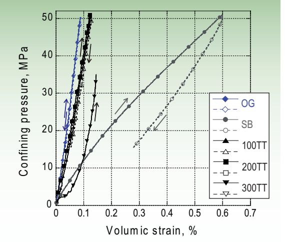

Fig. 8: *Mechanical data recorded under hydrostatic loading ($\varepsilon_{vol}=2\varepsilon_{rad}+\varepsilon_{ax}$).*

- Linear elastic mechanical behavior of OG, 100TT and 200TT

Permeability data on 300TT glass sample

For $P_{eff} \leq$ 10 MPa:

constant flow measurements

Darcy's law

$$k = \frac{Q}{\Delta P}\frac{L}{S}\mu$$

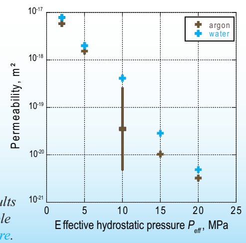

Fig. 9: *Permeability results obtained on 300TT sample under hydrostatic pressure.*

For $P_{eff} \geq$ 10 MPa:

1/2 pulse measurements

Brace et al., 1968

$$k = \alpha\beta\frac{L}{S}\mu V_{pulse}$$

- Permeability linearly drops on 4 orders up to diffusion
- No dependance of fluid nature (gas, liquid)

Deviatoric data

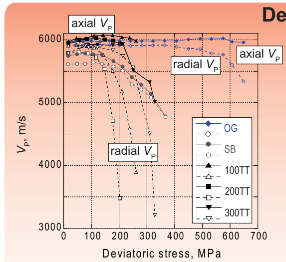

Fig. 10: *Average radial and axial P-wave velocities recorded under deviatoric loading.*

$$A = \frac{V_{Pax} - V_{Prad}}{V_{Pax}}$$

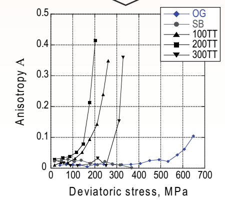

Fig. 11: *P-wave velocity anisotropy calculated for deviatoric loading (P_{conf}=15MPa).*

- OG rupture orientation parallel to the deviatoric stress.
- TT samples: the anisotropic mechanically induced cracks dominate over the initial thermal cracks.

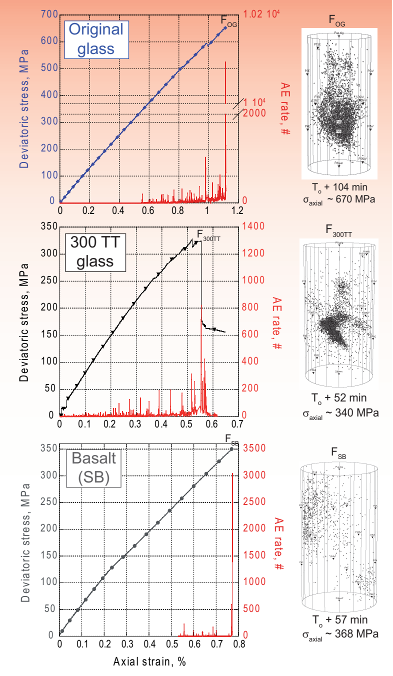

Fig. 12: *AEs rate correlated to the axial deformation under deviatoric loading (P_{conf}=15MPa).*

5. Interpretations & conclusions

Crack density ρ_c (penny-shape cracks assuming NIA) calculated following:
- Bristow (1960) and Walsh (1965) for overall isotropy;
- Kachanov (1994) and Sayers & Kachanov (1995) for anisotropic crack distribution (TI symmetry) in an isotropic medium.

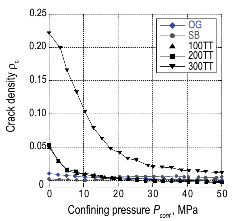

Fig. 13: *Thermal crack density evolution under hydrostatic loading.*

- Independent evidence for crack closure at $P_{eff} \leq$ 15 MPa
- Rare experimental data on percolation threshold

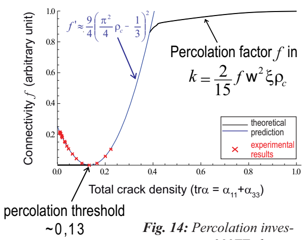

Fig. 14: *Percolation investigations on 300TT glass.*

Next steps:
- Direct correlation of crack density and permeability
- Thermochanical coupling effect on glass properties
- Stress corrosion investigations

- Strong influence of thermal treatement for ΔT=300°C on glass mechanical properties; minor influence for smaller thermal treatement temperatures.
- Close behavior of TT glasses and basalt.

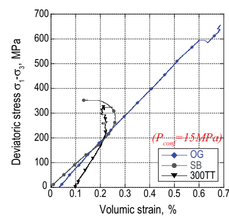

Fig. 15: *Mechanical behavior under deviatoric stress: evidence for dilatancy.*

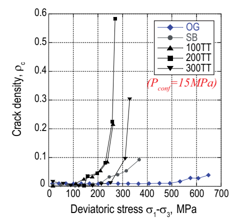

Fig. 16: *Total crack density calculated for damage under deviatoric stress.*

6. References

Frugier P., Gin S., Minet Y., Chave T., Bonin B., Godon N., Lartigue J., Jollivet P., Windt L.D. and Santarini G. (2008). SON68 nuclear glass dissolution kinetics: current state of knowledge and basis of the new graal model. Journal of Nuclear Materials, 380, 8–21.

Bristow J. (1960). Microcracks and the static and dynamic constants of annealed and heavily cold-worked metals. British Journal of Applied Physics, 11, 81–85.

Walsh J. (1965). The effect of cracks on the compressibility of rocks. JGR, 70, doi:10.1029/JZ070i002p00399

Sayers C. & Kachanov M. (1995). Microcracks-induced elastic wave anisotropy of brittle rocks. JGR, 100, 4149-4156

Guéguen Y. & Dienes J. (1989). Transport properties of rocks from statistics and percolation. Mathematical Geology, 21, pp. 13